Bull. Mater. Sci., Vol. 34, No. 7, December 2011, pp. 1385–1391. © Indian Academy of Sciences.

Effect of Mn doping on electrical properties and accelerated ageing behaviours of ternary ZVM varistors

C-W NAHM

Semiconductor Ceramics Laboratory, Department of Electrical Engineering, Dongeui University, Busan 614-714, Republic of Korea

MS received 20 June 2009; revised 22 January 2011

Abstract. The electrical properties and d.c. accelerated ageing behaviour of ZVM (Zn–V–Mn) ceramics were investigated with different valences and contents of Mn. The incorporation of Mn into the ZV ceramics was found to restrict the abnormal grain growth of ZnO. The nonlinear properties and stability against the d.c. accelerated ageing stress are significantly affected by different valences and contents of Mn. The high valence of Mn (Mn^{4+}) in the ZVM ceramics resulted in better nonlinear properties than low valence of Mn ($Mn^{2{\cdot}66+}$). Furthermore, an increase in doping level of MnO_2 greatly improved its nonlinear properties. The ZVM ceramics doped with 2 mol% MnO_2 exhibited not only a high nonlinearity, in which the nonlinear coefficient is 27 and the leakage current density is 0·042 mA/cm^2, but also a good stability, in which $\%\Delta E_{1\,mA} = -2{\cdot}1\%$, $\%\Delta\alpha = -25{\cdot}9\%$ for the d.c. accelerated ageing stress of 0·85 $E_{1\,mA}$/85°C/24 h.

Keywords. Mn-valence; microstructure; electrical properties; stability; Zn–V–Mn-based varistors.

1. Introduction

ZnO varistors are semiconducting electroceramic devices formed by sintering ZnO powder with minor dopants, such as Bi_2O_3, Pr_6O_{11} and CoO. They exhibit nonlinear electrical properties similar to back-to-back Si Zener diode. However, they have a much higher energy-handling capability. This nonlinear behaviour is due to the presence of a double Schottky barrier formed at the grain boundaries containing many trap states. Owing to high nonlinearity, the varistors are used widely in over-voltage protection systems in electronic circuits and electric power systems (Levinson and Philipp 1986; Gupta 1990). ZnO ceramics cannot exhibit a nonlinear behaviour without doping by heavy elements with large ionic radii such as Bi, Pr or Ba. Commercial Zn–B-based ceramics and Zn–Pr-based ceramics cannot be co-fired with a silver inner-electrode (m.p. 961°C) in multilayered chip components because of their relatively high sintering temperature above 1000°C (Matsuoka 1971; Alles and Burdvick 1991; Lee *et al* 1996; Chun *et al* 1999; Nahm *et al* 2000). Therefore, new varistor ceramics are required in order to use a silver inner-electrode. Of the varistor ceramics, one candidate is ZV (Zn–V) ceramics (Tsai and Wu 1994, 1996; Kuo *et al* 1998; Hng and Knowles 1999). The ZV ceramics can be sintered at a relatively low temperature in the vicinity of about 900°C. This is important for multilayer chip component applications, because it can be co-sintered with a silver inner-electrode without using expensive palladium or platinum metals.

To develop nonlinear ceramics of high performance, it is very important to comprehend the influences of additives on nonlinear properties (Nahm 2007). Mn is often doped with Zn–Bi-based ceramics to improve their varistor properties (Pike *et al* 1985; Freuter *et al* 1989). In this paper, the influence of the valences and contents of Mn on the microstructure, electric properties and d.c. accelerated ageing behaviour of the ZVM (Zn–V–Mn) ceramics is reported.

2. Experimental

2.1 *Sample preparation*

Reagent-grade raw materials were used in proportions of $(99{\cdot}5 - x)$ mol% ZnO, 0·5 mol% V_2O_5, x mol% Mn ions ($x = 0{\cdot}5$, 2·0). Mn ions were used in the oxide form such as $Mn^{2{\cdot}66+}$ (Mn_3O_4) and Mn^{4+} (MnO_2). Raw materials were mixed by ball-milling with zirconia balls and acetone in a polypropylene bottle for 24 h. The mixture was dried at 120°C for 12 h. The dried mixture was pulverized using an agate mortar/pestle after the addition of 0·8 wt% polyvinyl butyral (PVB) binder, it was granulated by sieving with a 100-mesh screen to produce the starting powder. The powder was uniaxially pressed into discs of 10 mm in diameter and 1·5 mm in thickness at a pressure of 80 MPa. The discs were covered with raw powder in alumina crucible, sintered at 900°C in air for

*Author for correspondence (cwnahm@deu.ac.kr)

3 h and furnace-cooled to room temperature. The sintered samples were lapped and polished to 1 mm thickness. The size of the final samples was about 8 mm in diameter and 1 mm in thickness. Silver paste was coated on both faces of the samples and the electrodes were formed by heating at 600°C for 10 min. The electrodes were 5 mm in diameter.

2.2 *Microstructure analysis*

Both sides of the samples were lapped and ground with SiC paper and polished with 0·3 μm-Al_2O_3 powder to a mirror-like surface. The polished samples were chemically etched at 1 $HClO_4$: 1000 H_2O for 25 s at 25°C. The surface of the samples was metallized with a thin coating of Au to reduce the charging effects and to improve the resolution of the image. The surface microstructure was examined by a scanning electron microscope (SEM, Hitachi S2400, Japan). The average grain size (d) was determined by the lineal intercept method using the expression, $d = 1{\cdot}56\,L/MN$ (Wurst and Nelson 1972), where L is the random line length on the micrograph, M is the magnification of the micrograph and N is the number of the grain boundaries intercepted by the lines. The compositional analysis of the selected areas was determined by an energy dispersion X-ray spectroscope (EDS) attached to the SEM unit. The crystalline phases were identified by powder X-ray diffractometer (XRD, Model *D*/max 2100, Rigaku, Japan) with CuKα radiation. The sintered density (ρ) was measured using a density determination kit (238490) attached to a balance (AG 245, Mettler Toledo International Inc., Greifensee, Switzerland).

2.3 *Electrical measurement*

The electric field–current density (E–J) characteristics were measured using a high-voltage source unit (Keithley 237, Keithley Instruments Inc., Cleveland, OH, USA). The breakdown field ($E_{1\,mA}$) was measured at 1 mA/cm^2 and the leakage current density (J_L) was measured at 0·8 $E_{1\,mA}$. In addition, the nonlinear coefficient (α) was defined by the empirical law, $J = KE^{\alpha}$, where J is the current density, E is the applied electric field and K is a constant. α was determined in the current density range 1–10 mA/cm^2, where $\alpha = 1/(\log E_2 - \log E_1)$ and E_1 and E_2 are the electric fields corresponding to 1·0 and 10 mA/cm^2, respectively.

The capacitance–voltage (C–V) characteristics of the samples were measured at 1 kHz, as a test frequency, using an RLC meter (QuadTech 7600, Marlborough, MA, USA) and an electrometer (Keithley 617, Keithley Instruments Inc., Cleveland, OH, USA). The donor concentration (N_d) and the barrier height (ϕ_b) were determined by the equation $(1/C_b - 1/2C_{bo})^2 = 2(\phi_b + V_{gb})/q\varepsilon N_d$, where C_b is the capacitance per unit area of a grain boundary, C_{bo} is the value of C_b when $V_{gb} = 0$, V_{gb} is the applied voltage per grain boundary, q is the electronic charge and ε is the permittivity of ZnO ($\varepsilon = 8{\cdot}5\varepsilon_0$) (Mukae *et al* 1979).

2.4 *D.C. accelerated ageing characteristic measurement*

The d.c. accelerated ageing stress test for the samples was performed under the stress state of 0·85 $E_{1\,mA}$/85°C/24 h. Simultaneously, the leakage current was monitored at intervals of 1 min during the stress test using a high-voltage source-measure unit (Keithley 237). The degradation rate coefficient (K_T) was calculated by the following expression $I_L = I_{Lo} + K_T t^{1/2}$, where I_L is the leakage current at stress time (t) and I_{Lo} is I_L at $t = 0$ (Fan and Freer 1994). After applying the respective stresses, the V–I characteristics were measured at room temperature.

3. Results and discussion

Figure 1 shows the SEM micrographs of the ZVM ceramics for different valences and contents of Mn. The samples doped with 0·5 mol% Mn content show very abnormal grain growth of ZnO. The nonuniformity of grain size was significantly reduced with an increase in the Mn content. With increasing Mn content, the average grain size decreased from 5·2 to 4·5 μm for the sample doped with Mn_3O_4 and it decreased from 8·4 to 5·2 μm for the sample doped with MnO_2. As a result, it can be seen that the increase of Mn content effectively reduced nonuniform and abnormal grain growth. Furthermore, it can be seen that different valences of Mn have an effect on the grain size. On the other hand, Mn doping did not significantly modify the densification process. The sintered density of the samples was in the range of 95·3–96% of the theoretical density for Mn_3O_4 and 94·6–95·3% of the theoretical density for MnO_2 (theoretical density for pure ZnO, 5·78 g/cm^3). The X-ray diffraction (XRD) patterns of the ZVM ceramics are shown in figure 2. The samples doped with Mn revealed the presence of $Zn_3(VO_4)_2$ as a secondary phase (Hng and Knowles 1999), in addition to the main hexagonal ZnO as a primary phase. Furthermore, the samples doped with Mn_3O_4 revealed additionally Mn-rich phase as a secondary phase, whereas no secondary phase related to MnO_2 was detected. $Zn_3(VO_4)_2$ is formed when ZV ceramics are sintered at a high temperature, which also acts as a liquid-phase sintering aid (Tsai and Wu 1994). The EDX microanalysis for the ZVM ceramics is shown in figure 3. No peak for the V species is found in the grain interior within the EDX detection limit, though the ion radius of V is smaller than that of Zn. This means that the V species are not dissolved into the ZnO grain. However, the Mn species was found to exist at the grain interior, in addition to Zn. On the other hand, it is found that the grain boundaries contain V and Mn species. As a result, the Mn species exist in both grain and grain boundaries. The more

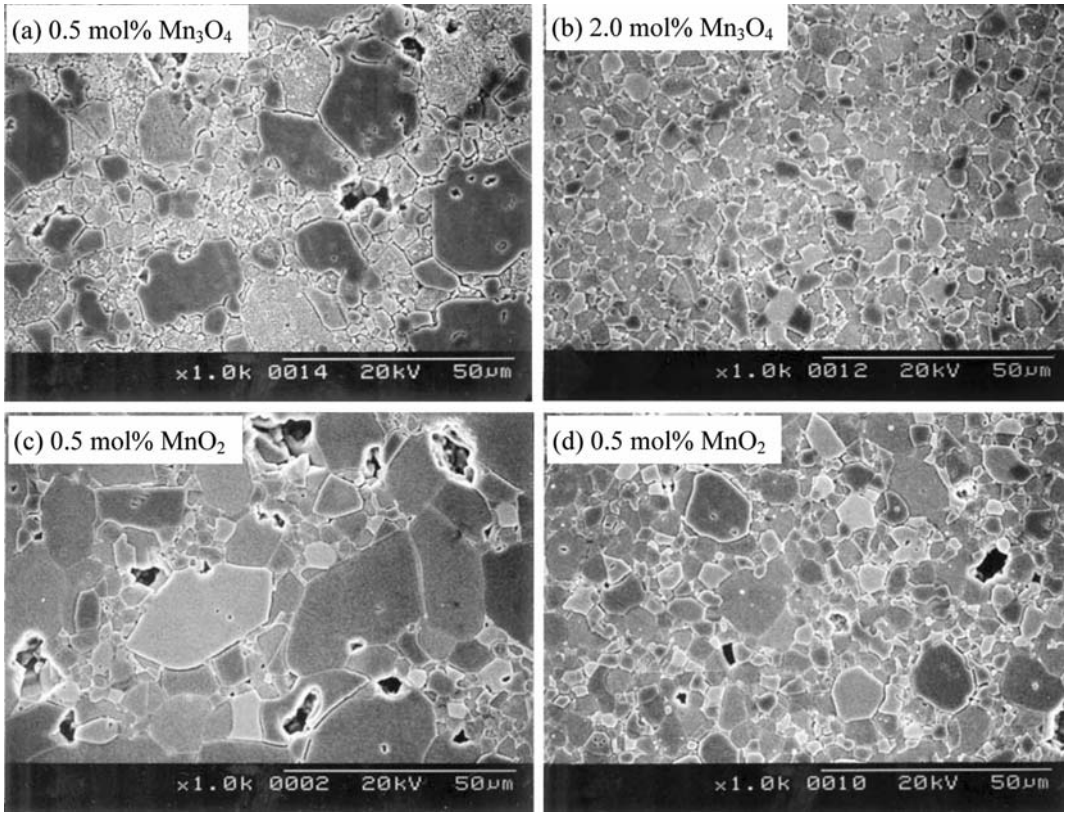

Figure 1. SEM micrographs of ZVM ceramics for different valences and contents of Mn.

Table 1. *E–J* characteristic parameters of ZVM ceramics for different valences and contents of Mn.

Dopant	Mn content (mol%)	d (μm)	ρ (g/cm^3)	$E_{1\,mA}$ (V/cm)	α	J_L (mA/cm^2)	N_d (10^{18} cm^{-3})	Φ_b (eV)
Mn_3O_4	0·5	5·2	5·51	1·072	20	0·17	0·43	2·66
	2·0	4·5	5·55	4·444	6	0·58	1·26	1·32
MnO_2	0·5	8·4	5·47	722	21	0·18	0·72	1·47
	2·0	5·2	5·51	999	27	0·042	0·18	1·99

detailed microstructural parameters are summarized in table 1.

Figure 4 shows the electric field–current density (*E–J*) characteristics of the ZVM ceramics for different valences and varied contents of Mn. It can be seen that the valences and contents of Mn have a significant effect on the conduction characteristics. The varistor properties are basically characterized by non-ohmicity in the *E–J* characteristics. The curves show the conduction characteristics dividing into an ohmic region before the breakdown and a non-ohmic region after the breakdown. The sharper the knee of the curves between the two regions, the better the non-ohmic properties. The samples doped with Mn_3O_4 revealed that the nonlinear properties are impaired with the increase of Mn_3O_4 content. On the contrary, the samples doped with MnO_2 revealed that the nonlinear properties are improved with the increase of MnO_2 content. As a result, the different valences and contents of Mn have a significant effect on nonlinear properties. The detailed electrical parameters are summarized in table 1.

The breakdown field ($E_{1\,mA}$) of the ZVM ceramics increased from 1072 to 4444 V/cm for the samples doped with Mn_3O_4 and from 722 V/cm to 999 V/cm for the samples doped with MnO_2 with the increase of Mn content. In general, the $E_{1\,mA}$ is firstly affected by the number of grain boundaries (n) across a series between the electrodes, which is inversely proportional to the average grain size. As a result, the decrease of the grain size leads to higher $E_{1\,mA}$. The $E_{1\,mA}$ is in turn affected by the breakdown voltage per grain boundary (v_{gb}), as expressed by the following equation (Levinson and Phillip 1986): $E_{1\,mA} = v_{gb}/d$, where d is the grain size. As a result, the

increase of the v_{gb} leads to higher $E_{1\,mA}$. It can be seen from the equation that the decrease of average grain size with the increase of Mn content will increase $E_{1\,mA}$. The nonlinear coefficient (α) values are derived from the E–J curves. It was reported that the α-value of the binary ZV ceramics was less than 5 (Tsai and Wu 1994), whereas the α-value of the ZVM ceramics extremely improved when Mn was doped. The samples doped with Mn_3O_4 ranked the highest in α (20) in 0·5 mol% content. However, the excessive doping levels of Mn_3O_4 abruptly impaired it. This is attributed to a poor grain boundary, which exhibits a very low electrostatic potential barrier. As a result, the Mn_3O_4-doped samples exhibited very poor electrical properties due to their bad grain boundaries. On the other hand, the samples doped with MnO_2 exhibited higher α from 21 to 27 with the increase of Mn content. The maximum of nonlinear coefficient (27) was obtained for the samples doped with 2 mol% MnO_2. It should be noted that MnO_2 provides higher α than that of Mn_3O_4. It should be noted that the nonlinear coefficient higher than 27 in the ZVM ceramics is much higher than the nonlinear coefficient (13–18) for ternary system ZnO–Bi–CoO (or MnO) ceramics (Matsuoka 1971). As a result, the samples doped with 2 mol% MnO_2 could be applied to low-voltage varistors because of low breakdown voltage per grain boundary and high nonlinear coefficient. On the other hand, the variation of leakage current density (J_L) is entirely different for different valences and contents of Mn. These behaviours are opposite to the variation of the nonlinear coefficient. That is, the high α leads to the low J_L. As a result, the samples doped with MnO_2 exhibited markedly better nonlinear electrical properties than the samples doped with Mn_3O_4. Furthermore, the nonlinear properties were improved with the increase of MnO_2 content. The more detailed E–J characteristic parameters are summarized in table 1.

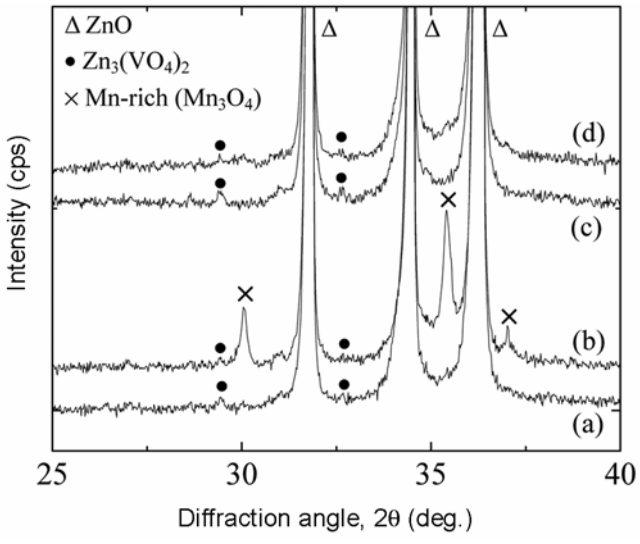

Figure 2. XRD patterns of ZVM ceramics for different valences and contents of Mn: (a) 0·5 mol% Mn_3O_4, (b) 2 mol% Mn_3O_4, (c) 0·5 mol% MnO_2 and (d) 2 mol% MnO_2.

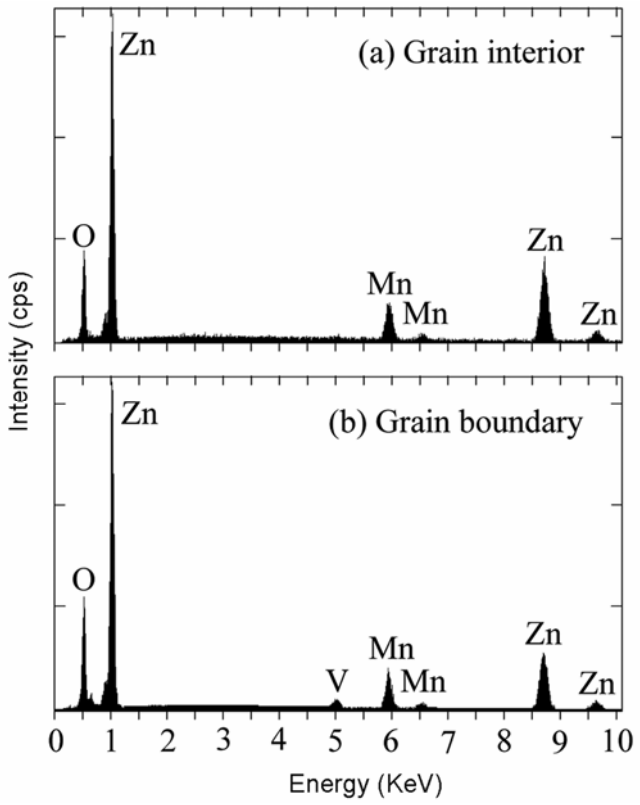

Figure 3. EDX analysis of ZVM ceramics.

Figure 5 shows the capacitance–voltage (C–V) characteristics of the ZVM ceramics for different valences and contents of Mn. It can be seen that the modified C–V plotting curves are almost linear and they are affected by different valences and contents of Mn. The C–V parameters such as the donor density (N_d) and barrier height (ϕ_b) are basically derived from figure 5 and are summarized in table 1. The N_d value with the increase in Mn_3O_4 content increased from $0{\cdot}43 \times 10^{18}$ cm^{-3} to $1{\cdot}26 \times 10^{18}$ cm^{-3}, whereas it decreased from $0{\cdot}72 \times 10^{18}$ cm^{-3} to $0{\cdot}18 \times 10^{18}$ cm^{-3} with the increase in MnO_2 content. This shows that Mn species can act as an acceptor or a donor with different valence states. The increase of N_d value with the increase of Mn_3O_4 content can be explained as follows. V_2O_5 is usually an oxidizing agent and it may convert Mn_3O_4 to MnO_2 ($Mn_3O_4 + O_2 \rightarrow 3MnO_2$). Thus, it is presumed that the incorporation of Mn_3O_4 reduces ZnO–V_2O_5 system. The N_d value is related to the partial pressure of oxygen (P_{O_2}), namely, $N_d \propto P_{O_2}^{-1/4}$ or $P_{O_2}^{-1/6}$ (Mahan 1983; Yan and Heuer 1983). It is, therefore, believed that the increase of donor concentration with the increase of Mn_3O_4 content is associated with a decrease of partial pressure of oxygen in the materials. By contrast, the decrease of N_d value with the increase of MnO_2 content follows opposite process in the case of Mn_3O_4. The ϕ_b value with the increase of Mn_3O_4 content decreased from 2·66 to 1·32 eV, whereas it increased from 1·47 to 1·99 eV with the increase of MnO_2

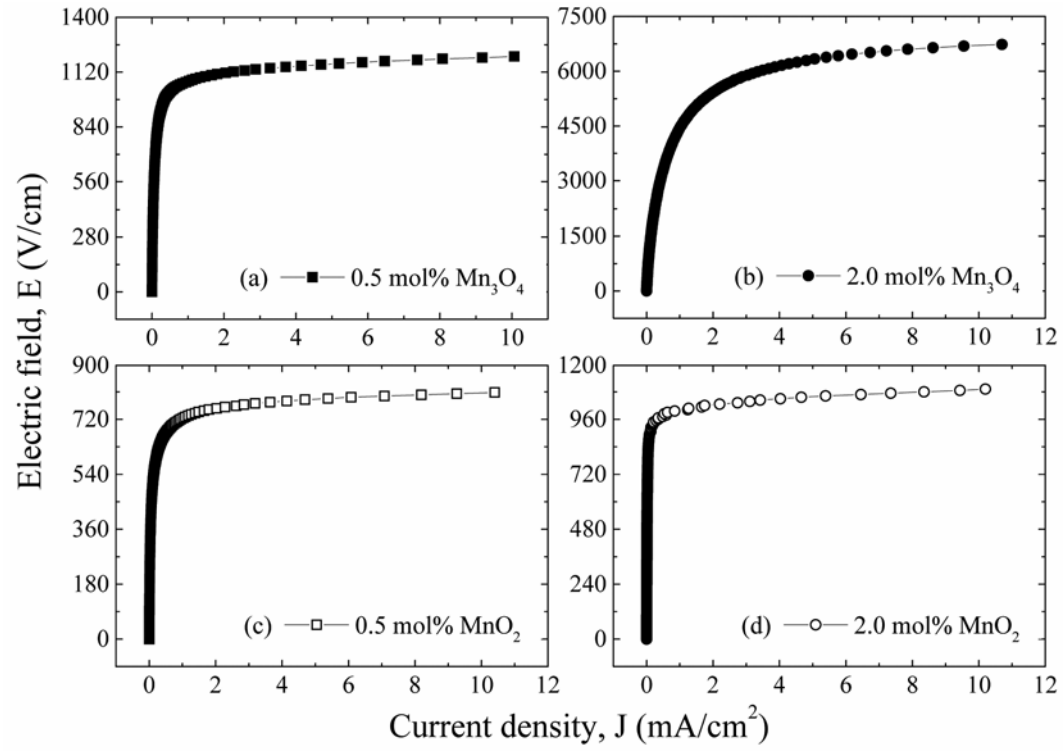

Figure 4. *E–J* characteristics of ZVM ceramics for different valences and contents of Mn.

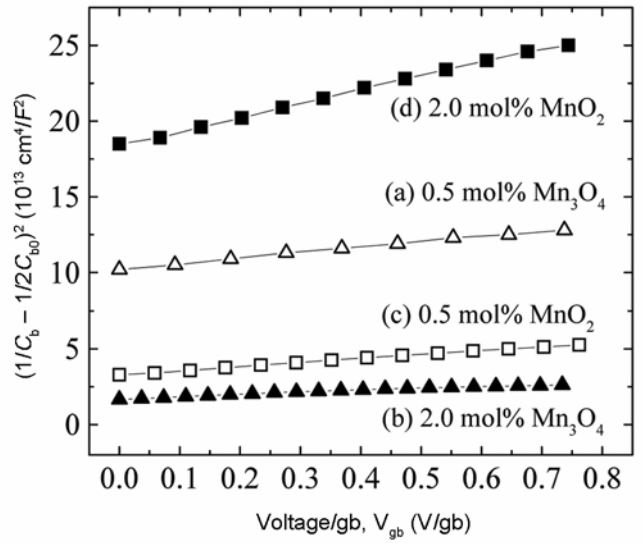

Figure 5. *C–V* characteristics of ZVM ceramics for different valences and contents of Mn.

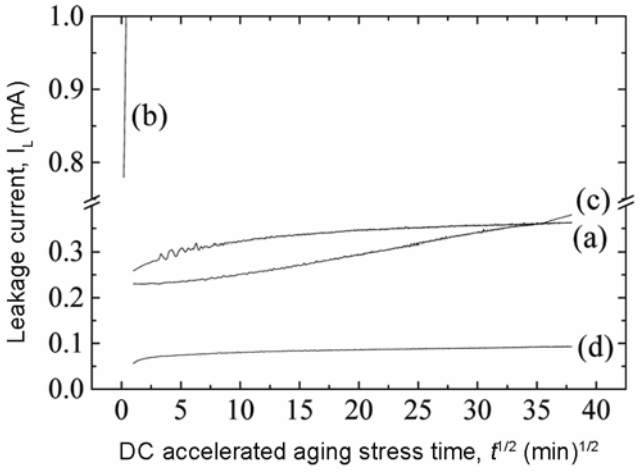

Figure 6. Leakage current during applying the d.c. accelerated ageing stress of ZVM ceramics for different valences and contents of Mn: (a) 0·5 mol% Mn_3O_4, (b) 2 mol% Mn_3O_4, (c) 0·5 mol% MnO_2 and (d) 2 mol% MnO_2.

content. Overall variation of ϕ_b value with the increase of Mn content showed the opposite variation to N_d value. The variation of ϕ_b coincides with that of α in *E–J* characteristics. That is, the high ϕ_b gives rise to the high α in terms of the conduction mechanism.

Electrical and electronic devices begin to degrade because of gradually increasing leakage current with stress time. For the varistors, in addition to nonlinear properties, the electrical stability is a technologically very important characteristic of systems.

Figure 6 shows the leakage current (I_L) behaviour of the ZVM ceramics for different valences and contents of Mn during applying the d.c. accelerated ageing stress of 0·85 $E_{1\,mA}$/85°C/24 h. The I_L gradually increased with increasing stress time, and this shows that the samples are gradually degraded. The stability of ceramics can be estimated by the degradation rate coefficient (K_T), indicating the degree of ageing. This exhibits the slope of leakage current against the stress time. The lower K_T leads to the higher stability. The samples doped with 0·5 mol%

Table 2. Variation of *E–J* characteristics before and after applying the d.c. accelerated ageing stress of ZVM ceramics for different valences and contents of Mn.

Dopant	Mn content (mol%)	Stress state	K_T ($\mu A\ h^{-1/2}$)	$E_{1\ mA}$ (V/cm)	$\%\Delta E_{1\ mA}$	α	$\%\Delta\alpha$	J_L (mA/cm^2)	$\%\Delta J_L$
Mn_3O_4	0·5	Initial		1072		20		0·17	
		Stressed	12·0	960	–10·4	11	–45·0	0·48	182·3
	2·0	Initial		4444		6		0·58	
		Stressed	Thermal runaway	2556	–42·5	3	–50·0	0·74	27·6
MnO_2	0·5	Initial		722		21		0·18	
		Stressed	35·3	502		5		0·62	244·4
	2·0	Initial		999		27		0·042	
		Stressed	3·8	978	–2·1	20	–25·9	0·21	400

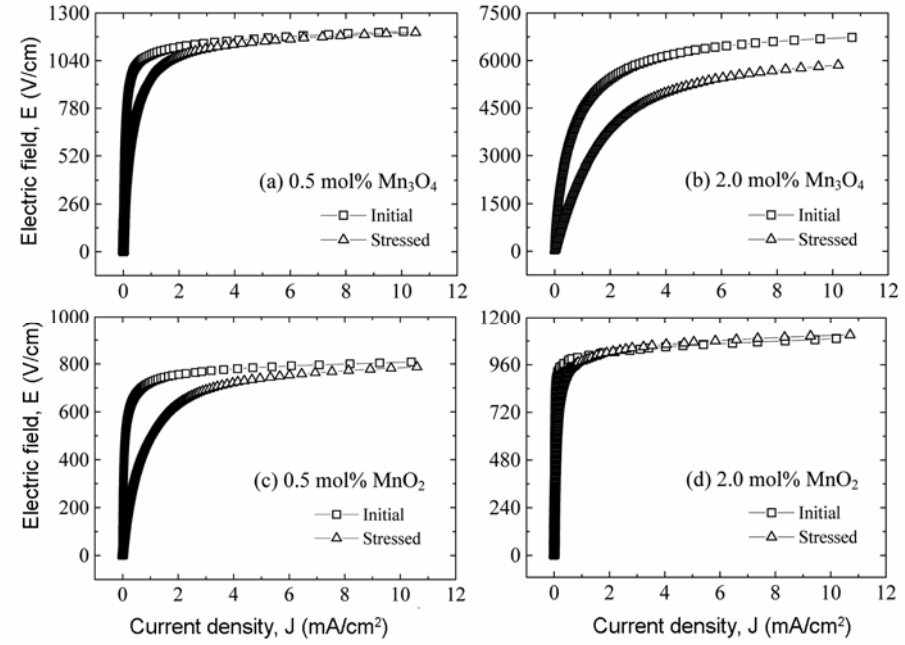

Figure 7. Variation of *E–J* characteristics before and after applying the d.c. accelerated ageing stress of ZVM ceramics for different valences and contents of Mn.

Mn_3O_4 were relatively stable possessing a K_T value of 12 $\mu A\ h^{-1/2}$. However, the samples doped with 2 mol% Mn_3O_4 caused thermal runaway. On the other hand, the samples doped with MnO_2 exhibited good stability without thermal runaway. In particular, the samples doped with 2 mol% MnO_2 exhibited the best stability possessing a K_T value of 3·8 $\mu A\ h^{-1/2}$.

In discussing the stability macroscopically, the sintered density and leakage current have a significant effect on stability. The low sintered density decreases the number of parallel conduction paths and eventually leads to the concentration of current. The high leakage current gradually increases the carrier generation due to Joule heat and it leads to repetition cycle between Joule heating and leakage current. This is core for ageing mechanism from a macroscopic viewpoint. In the light of these facts, it seems that the electrical stability of these ZVM ceramics against the d.c. accelerated ageing stress is affected by more leakage current than sintered density. As a result, it can be seen that the resistance against the d.c. accelerated ageing stress is greatly affected by the valances and contents of Mn.

Figure 7 shows the *E–J* characteristic behaviour before and after applying the d.c. accelerated ageing stress of the ZVM ceramics for different valences and contents of Mn. It can be seen that the variation of *E–J* curves after applying the stress is strongly affected by different valences and contents of Mn. On the whole, the variation of *E–J*

curves after applying the stress of the ZVM ceramics coincided with the K_T value. Of the samples, the sample doped with 2 mol% MnO_2 exhibited a smallest variation in E–J curves. There is no variation of the curve at low and high current regimes except for the vicinity of knee. The variations of E–J characteristics before and after applying the stress are summarized in table 2.

The $E_{1\,mA}$ and α values of all the ZVM ceramics after applying the stress decreased, compared with those before applying the stress. The samples doped with 2 mol% MnO_2 exhibited a low variation rate, only –2·1% in $\Delta E_{1\,mA}$, whereas relatively large variation rate, –25·9% in $\Delta\alpha$. However, the α value was maintained at the high value of 20 after applying the stress.

4. Conclusions

The influence of valences and contents of Mn on electrical properties and d.c. accelerated ageing behaviour of the ZVM ceramics was investigated. For all samples, the microstructure of the ZVM ceramics commonly consisted of ZnO grain as a primary phase and $Zn_3(VO_4)_2$ as a secondary phase. The incorporation of Mn dopant to the binary ZV ceramics was found to restrict abnormal grain growth of ZnO. The high valence of Mn (Mn^{4+}) has a better effect on nonlinear properties than the low valence ($Mn^{2\cdot66+}$). The samples doped with 2 mol% MnO_2 exhibited not only a high nonlinearity, with nonlinear coefficient of 27 and leakage current density of 0·042 mA/cm^2, but also a good stability, in which $\%\Delta E_{1\,mA} = -2\cdot1\%$, $\%\Delta\alpha = -25\cdot9\%$ for the d.c. accelerated ageing stress of 0·85 $E_{1\,mA}$/85°C/24 h. Conclusively, it was estimated that the ternary ZnO–0·5 mol% V_2O_5–2 mol% MnO_2-based ceramics is a potential material for multilayer chip varistors with a silver inner-electrode.

References

Alles A B and Burdick V L 1991 *J. Appl. Phys.* **70** 6883

Chun S Y, Shinozaki K and Mizutani N 1999 *J. Am. Ceram. Soc.* **82** 3065

Fan J and Freer R 1994 *J. Am. Ceram. Soc.* **77** 2663

Greuter F, Latter G, Rossineli M and Stucki F 1989 *Advances in varistor technology* (Westerville, OH: American Ceramic Society) p. 31

Gupta T K 1990 *J. Am. Ceram. Soc.* **73** 1817

Hng H H and Knowles K M 1999 *J. Eur. Ceram. Soc.* **19** 721

Kuo C T, Chen C S and Lin I N 1998 *J. Am. Ceram. Soc.* **81** 2942

Lee Y S, Liao K S and Tseng T Y 1996 *J. Am. Ceram. Soc.* **79** 2379

Levinson L M and Philipp H R 1986 *Am. Ceram. Soc. Bull.* **65** 639

Mahan G D 1983 *J. Appl. Phys.* **75** 3825

Matsuoka M 1971 *Jpn. J. Appl. Phys.* **10** 736

Mukae M, Tsuda K and Nagasawa I 1979 *J. Appl. Phys.* **50** 4475

Nahm C W 2007 *J. Mater. Sci.* **42** 8370

Nahm C W, Park C H and Yoon H S 2000 *J. Mater. Sci. Lett.* **19** 271

Pike G S, Kurtz S R, Gourley P L, Philipp H R and Levinson L M 1985 *J. Appl. Phys.* **57** 5512

Tsai J K and Wu T B 1994 *J. Appl. Phys.* **76** 4817

Tsai J K and Wu T B 1996 *Mater. Lett.* **26** 199

Wurst J C and Nelson J A 1972 *J. Am. Ceram. Soc.* **55** 109

Yan M F and Heuer A H 1983 *Additives and interfaces in electronic ceramics* (*Am. Ceram. Soc. Columbus OH*) p. 71